Université Pierre et Marie Curie

Master Sciences et Technologie (M2)

Spécialité : Concepts fondamentaux de la physique

Parcours : Physique des Liquides et Matière Molle

Cours : Dynamique Non-Linéaire

Laurette TUCKERMAN

laurette@pmmh.espci.fr

Quasiperiodicity and Intermittency

English-language version

Quasiperiodicity and Intermittency

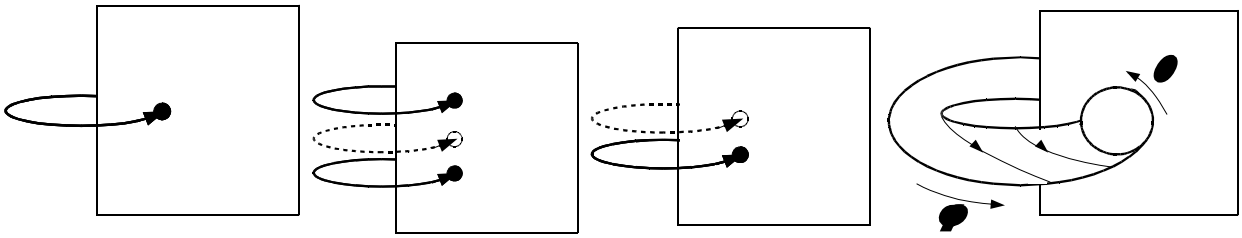

Figure 1: Poincaré sections of flows containing limit cycles. From left to right: before any bifurcation, after a pitchfork bifurcation, afer a saddle-node bifurcation, after a Hopf bifurcation.

A system undergoes a Hopf bifurcation (or other event) creating a limit cycle. The limit cycle then undergoes another a Hopf bifurcation. If we consider the discrete first return or Poincaré map, the limit cycle is a fixed point and it undergoes a Hopf bifurcation. For the original continuous dynamical system, this is called a secondary Hopf or a Neimark Sacker bifurcation and leads to a torus, as shown in the rightmost portion of figure 1. Trajctories wind around the torus.

Circle maps

For the Poincaré map, the unstable fixed point is now surrounded by an *invariant circle*. The discrete trajectories do not go around the circle continually, but jump from point to point. This motivates the study of *circle maps*:

$$\theta_{n+1} = f(\theta_n) \mod 1 \tag{1}$$

(In this chapter, angles are measured in units of 2π radians.)

The basic prototype for a circle map is the *sine circle map* studied by V. Arnold in the 1960s (then at Moscow, now also at University of Paris IX, Dauphine):

$$\theta_{n+1} = f_{\Omega,K}(\theta_n) \equiv \left[\theta_n + \Omega - \frac{K}{2\pi}\sin(2\pi\theta_n)\right] \mod 1 \tag{2}$$

The parameter K measures the strength of a nonlinear perturbation. We start by giving the behavior of the sine circle map (2) for the linear case of $K = 0$. The behavior depends on Ω, which is the basic frequency of the map.

If	$\Omega = 0$	then	all θ are fixed points of f
If	$\Omega = p$ any integer		all θ are fixed points of f
If	$\Omega = p/q$	then	all θ are members of q-cycles of f
			$f^q(\theta) = [\theta + \underbrace{\frac{p}{q} + \frac{p}{q} + \ldots \frac{p}{q}}_{q \text{ times}}] \mod 1 = [\theta + p] \mod 1 = \theta$
If	Ω irrational	then	there are *no* fixed points or q-cycles
			All θ are members of *quasiperiodic orbits*
			Each orbit is dense on the circle

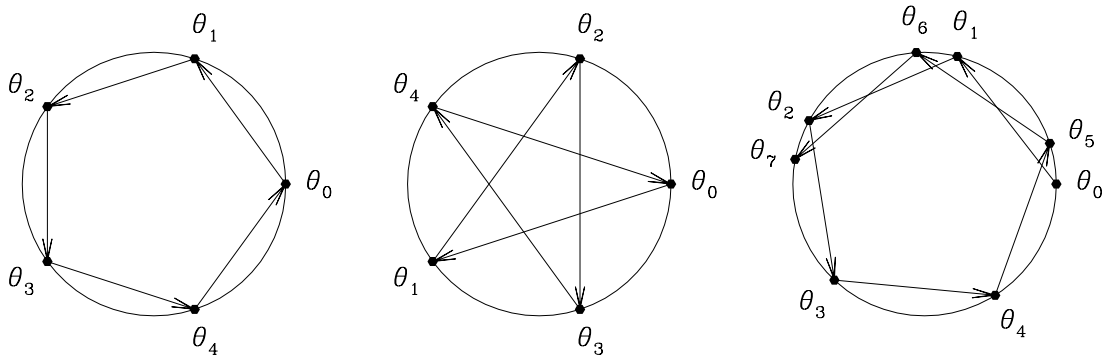

Figure 2: Trajectories of circle map $\theta_{n+1} = \theta_n + \Omega$ for $\Omega = 1/5$, $\Omega = 3/5$ and for Ω slightly more than 1/5. Since the map is discrete, trajectories are not continuous and may traverse the circle non-monotonically. When $\Omega = 3/5$, the trajectory is a 5-cycle which goes around the circle 3 times. If Ω is irrational, the trajectory contains an infinite number of points and never closes on itself.

Frequency locking

We now turn our attention to the nonlinear case $K \neq 0$ (within the range $0 \leq K < 1$). Figure 3 shows a circle map that has undergone a saddle-node bifurcation, creating a stable and unstable fixed point. For the original flow, this corresponds to the creation of a stable and unstable limit cycle. This phenomenon is called frequency locking.

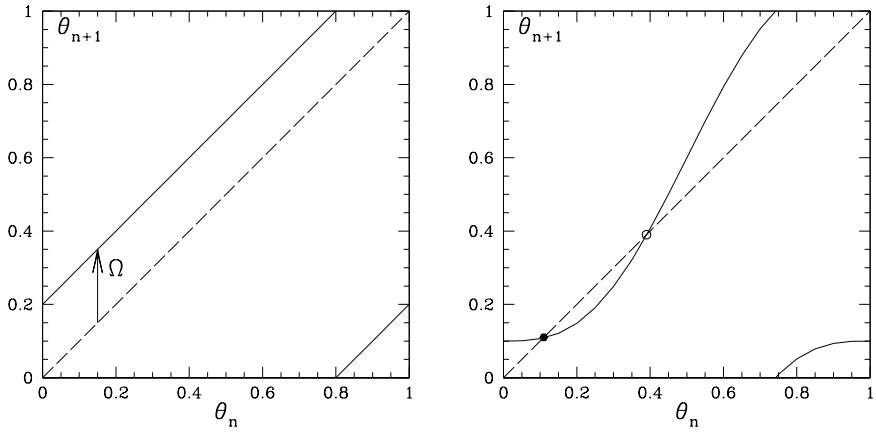

Figure 3: Sine circle map. Left: for $K = 0$, $f(\theta) = \theta + \Omega$. Right: for $K > 0$, a saddle-node bifurcation may create a pair of fixed points, one stable and one unstable. Values are $(\Omega, K) = (0.2, 0)$ (left) and (0.1,1) (right).

Let us determine some cycles and bifurcation points for the sine circle map. We seek points such that

$$f'(\theta) = 1 \qquad f(\theta) = \theta \tag{3}$$

$$1 - K\cos(2\pi\theta) = 1 \qquad \theta + \Omega - \frac{K}{2\pi}\sin(2\pi\theta) = \theta + n \tag{4}$$

$$\cos(2\pi\theta) = 0 \qquad \sin(2\pi\theta) = \frac{2\pi}{K}(\Omega - n) \tag{5}$$

$$\theta = \frac{1}{4} \implies \sin\left(2\pi\frac{1}{4}\right) = 1 = \frac{2\pi}{K}\Omega \implies K = 2\pi\Omega \tag{6}$$

$$\theta = \frac{3}{4} \implies \sin\left(2\pi\frac{3}{4}\right) = -1 = \frac{2\pi}{K}(\Omega - 1) \implies K = 2\pi(1 - \Omega) \tag{7}$$

Figure 4 shows the saddle-node bifurcations taking place at $\theta = 1/4$, $K = 2\pi\Omega$ and $\theta = 3/4$, $K = 2\pi(1-\Omega)$. Figure 5 shows the two bifurcation curves in the (Ω, K) plane, For $0 < \Omega < K/(2\pi)$, (left portion of figure 5) or $1 - K/(2\pi) < \Omega < 1$ (right portion of figure 5), the sine circle map has a pair of fixed points, while for $K/(2\pi) < \Omega < 1 - K/(2\pi)$, it has no fixed points.

Having found fixed points, i.e. one-cycles, we now seek two-cycles. The sine circle map does not undergo any period-doubling bifurcation in the range $0 < K < 1$ since, as shown on figure 6, $1 - K < f'(\theta) < 1 + K$, so $f'(\theta)$ is never negative in this range. Thus, two-cycles cannot appear via period-doubling bifurcations of f, which, we recall, are pitchfork bifurcations of the second iterate $f^2 \equiv f(f(\theta))$. Two-cycles can and do, however, appear via saddle-node bifurcations of f^2. Since $f_{(\Omega=1/2,K=0)}$ is a map for which all θ's are members of two-cycles, we write

$$\Omega_\pm(K) = \frac{1}{2} \pm \epsilon(K) \tag{8}$$

with K, $\epsilon(K)$ small. We write the form of the second iterate f^2 as:

$$\begin{array}{rcccccc} f^2(\theta) & = & f(\theta) & + & \Omega_\pm(K) & - & \frac{K}{2\pi}\sin(2\pi f(\theta)) \\ & = & \theta + \frac{1}{2} \pm \epsilon(K) - \frac{K}{2\pi}\sin(2\pi\theta) & + & \frac{1}{2} \pm \epsilon(K) & - & \frac{K}{2\pi}\sin(2\pi f(\theta)) \\ & = & \theta + 1 \pm 2\epsilon(K) - \frac{K}{2\pi}\sin(2\pi\theta) & & & - & \frac{K}{2\pi}\sin(2\pi f(\theta)) \end{array} \tag{9}$$

We expand the last term in (9) as:

$$\begin{aligned} \sin(2\pi f(\theta)) &= \sin\left(2\pi\left(\theta + \frac{1}{2} \pm \epsilon(K) - \frac{K}{2\pi}\sin(2\pi\theta)\right)\right) \\ &= \sin\left(2\pi\theta + \pi \pm 2\pi\epsilon - K\sin(2\pi\theta)\right) \\ &= \underbrace{\sin(2\pi\theta + \pi)}_{=-\sin(2\pi\theta)}\underbrace{\cos\left(\pm 2\pi\epsilon - K\sin(2\pi\theta)\right)}_{\approx 1} + \underbrace{\cos(2\pi\theta + \pi)}_{=-\cos(2\pi\theta)}\underbrace{\sin\left(\pm 2\pi\epsilon - K\sin(2\pi\theta)\right)}_{\approx \pm 2\pi\epsilon - K\sin(2\pi\theta)} \\ &\approx -\sin(2\pi\theta) - \cos(2\pi\theta)\left(\pm 2\pi\epsilon - K\sin(2\pi\theta)\right) \end{aligned} \tag{10}$$

where we have used $\sin(\theta+\pi) = -\sin(\theta)$, $\sin\epsilon \approx \epsilon$, $\cos(\theta+\pi) = -\cos(\theta)$, and $\cos\epsilon \approx 1$. Substituting (10) into (9), we obtain

$$\begin{aligned} f^2(\theta) &\approx \theta + 1 \pm 2\epsilon - \frac{K}{2\pi}\sin(2\pi\theta) - \frac{K}{2\pi}\left(-\sin(2\pi\theta) - \cos(2\pi\theta)\left(\pm 2\pi\epsilon - K\sin(2\pi\theta)\right)\right) \\ &= \theta + 1 \pm 2\epsilon + \frac{K}{2\pi}\cos(2\pi\theta)\left(\pm 2\pi\epsilon - K\sin(2\pi\theta)\right) \end{aligned} \tag{11}$$

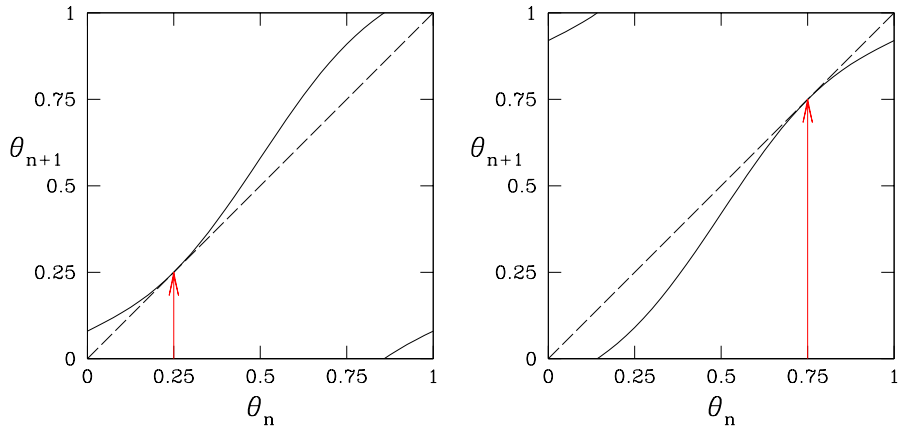

Figure 4: Saddle-node bifurcations of sine circle map f at $K = 0.5$.
At $\Omega = K/(2\pi) = 0.08$, a stable-unstable pair of fixed points is created/destroyed at $\theta = 1/4$.
At $\Omega = 1 - K/(2\pi) = 0.92$, a stable-unstable pair of fixed points is created/destroyed at $\theta = 3/4$.

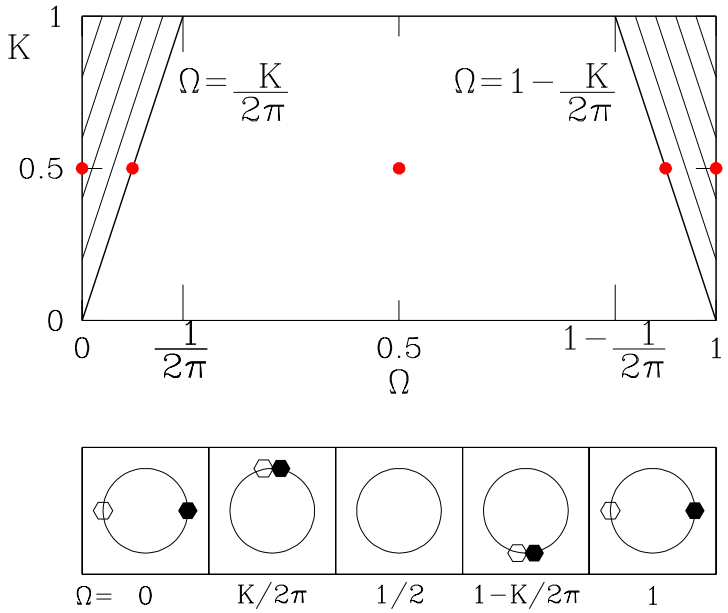

Figure 5: First frequency-locking tongue in (Ω, K) plane. Fixed points (one-cycles) exist inside the tongue, i.e. for $0 \leq \Omega < K/(2\pi)$ and $1 - K/(2\pi) < \Omega \leq 1$.

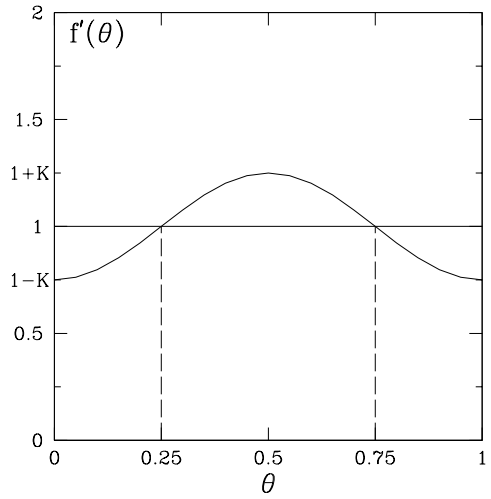

Figure 6: Derivative $f'(\theta)$ of sine circle map for $K = 0.25$. $1 - K \leq f' \leq 1 + K$ and $f'(\theta) = 1$ for $\theta = 1/4, 3/4$. $f'(\theta)$ is positive for all θ if $K < 1$.

We seek fixed points of $f^2(\theta) \mod 1$:

$$\begin{aligned} 0 = (f^2(\theta) - \theta) \mod 1 &\approx \pm 2\epsilon + \frac{K}{2\pi}\cos(2\pi\theta)\,(\pm 2\pi\epsilon - K\sin(2\pi\theta)) \\ = \pm 2\epsilon\,(1 + K\cos(2\pi\theta)) &- \frac{K^2}{2\pi}\cos(2\pi\theta)\sin(2\pi\theta) \end{aligned} \tag{12}$$

The terms in (12) are of order ϵ, ϵK and K^2. Since $\epsilon K \ll \epsilon$, the balance must be between terms of order ϵ and K^2:

$$\epsilon \approx \pm\frac{K^2}{8\pi}\sin(4\pi\theta) \tag{13}$$

The saddle-node bifurcations of f^2 and the bifurcation curves in the (Ω, K) parameter plane are plotted in in figures 7 and 8. As we did for the one-cycles, the condition

$$\frac{d}{d\theta} f^2(\theta) = 1 \tag{14}$$

can be used to determine θ. It turns out that the values of θ are near 1/8, 3/8, 5/8, 7/8.

Just as one-cycles occur via saddle-node bifurcations of f and two-cycles via saddle-node bifurcations of f^2, three-cycles emerge from $K = 0$, $\Omega = 1/3$ and $\Omega = 2/3$ via saddle-node bifurcations of f^3. These three-cycles exist over Ω-intervals of width $O(K^3)$. In general, for any integers p, q, we can seek Ω, K, θ satisfying

$$f^q_{\Omega,K}(\theta) = \theta + p \tag{15}$$

where we *do not* use use mod 1 to construct f^q (in order to retain knowledge of the value of p). Such cycles are created via saddle-node bifurcations and exist over a finite interval of (Ω, K). These regions are called *frequency-locking tongues* or *Arnold tongues*. The union of all such tongues has zero measure (consisting of the rationals $\Omega = p/q$) at $K = 0$ and widen as K increases. At $K = 1$ the union of the tongues has measure one.

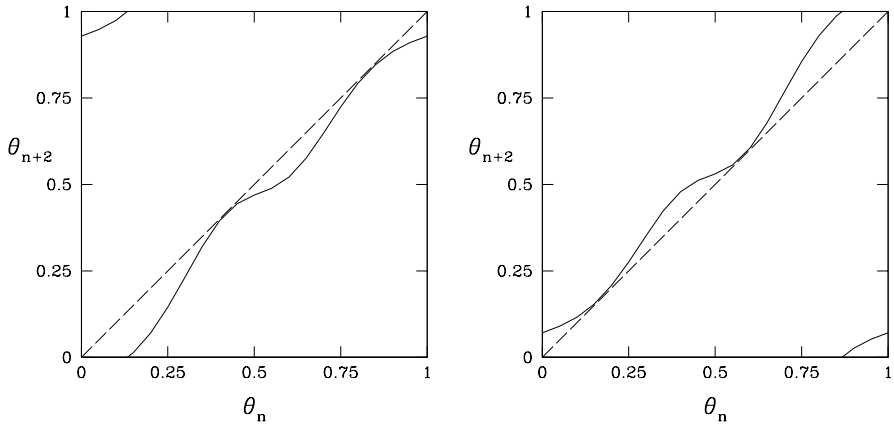

Figure 7: Saddle-node bifurcations of second iterate f^2 of sine circle map at $K = 0.5$.
At $\Omega \approx 1/2 - K^2/(8\pi) \approx 0.475$, two stable-unstable pairs of fixed points are created/destroyed at $\theta \approx 3/8$ and 7/8. At $\Omega \approx 1/2 - K^2/(8\pi) \approx 0.525$, two stable-unstable pairs of fixed points are created/destroyed at $\theta \approx 1/8$ and 5/8.

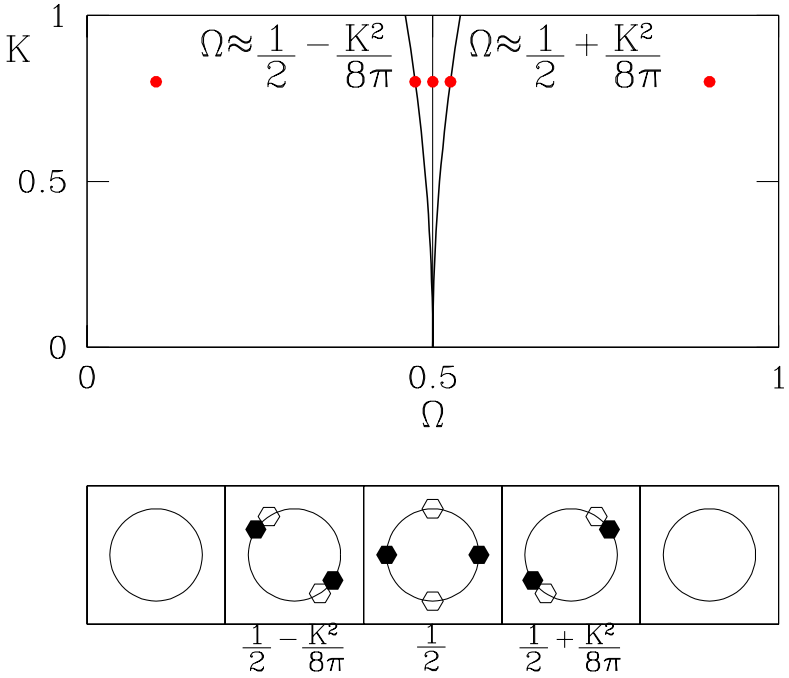

Figure 8: Frequency-locking tongue 1/2 in (Ω, K) plane. Two-cycles exist inside the tongue, i.e. for $1/2 - K^2/(8\pi) \lesssim \Omega \lesssim 1/2 + K^2/(8\pi)$.

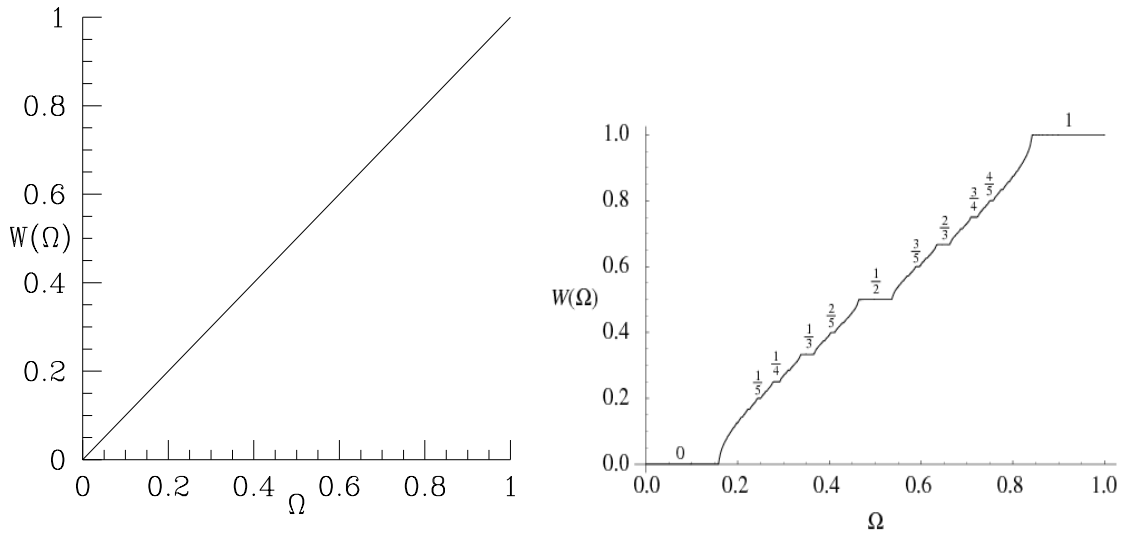

Figure 9: Winding number $W(f_{\Omega,K})$ for $K = 0$ (left, simple diagonal line) and for $K = 1$ (right, devil's staircase) Devil's staircase from E. Weisstein, MathWorld, `http://mathworld.wolfram.com/DevilsStaircase.html`.

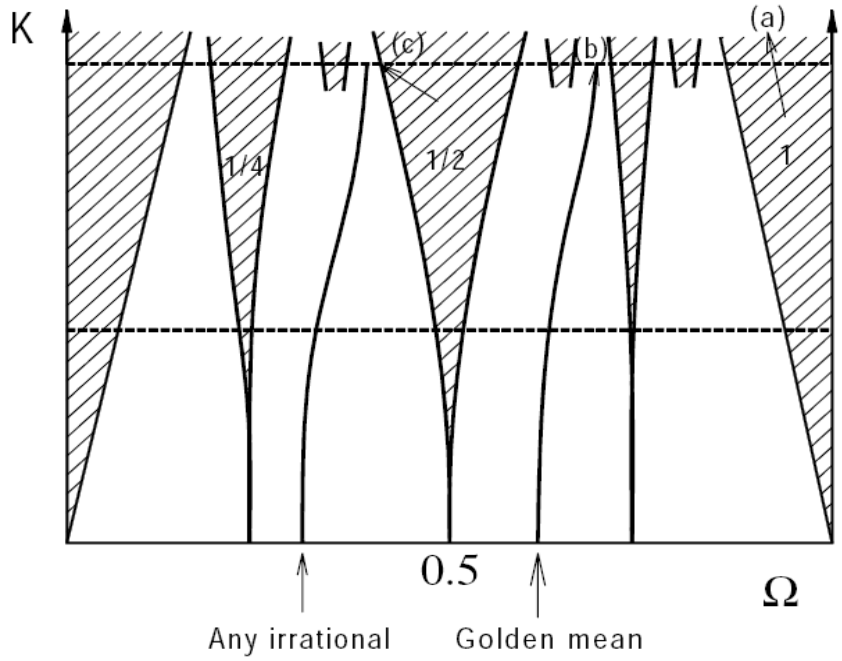

Figure 10: Schematic representation of frequency locking tongues in the (Ω, K) plane. From M. Cross, CalTech, `http://www.cmp.caltech.edu~mcc/Chaos_Course/Lesson19/Circle.pdf`

Winding number

We define the *winding number* of a circle map f to be

$$W(f) \equiv \lim_{n\to\infty} \frac{f^n(\theta_0) - \theta_0}{n} \tag{16}$$

where f^n is *not* truncated to $[0, 1]$. Poincaré showed that if f is monotonic and continuous, then this limit exists and is independent of θ_0. For the sine circle map with $K = 0$,

$$W(f_{\Omega,K=0}) \equiv \lim_{n\to\infty} \frac{\theta_0 + n\Omega - \theta_0}{n} = \Omega \tag{17}$$

The winding number generalizes the frequency Ω to maps which are less trivial. In particular, when (Ω, K) is inside a frequency-locking tongue with frequency p/q, then $W(f_{\Omega,K}) = p/q$. Thus, from figures 5 and 8, we see that $W(f_{\Omega=0,K}) = 0$, $W(f_{\Omega=1/2,K}) = 1/2$ and $W(f_{\Omega=1,K}) = 1$ for all K.

At $K = 1$, the graph of $W(f_{\Omega,K=1})$ is called the Devil's staircase and is shown in figure 9. It consists of a series of steps, with narrow steps for large denominators q and wide steps for small denominators q. It is continuous (!) and constant almost everywhere (on a set of measure one), with jumps at each irrational number.

The golden mean

The "most irrational"number, which is the golden mean, stays furthest away from the frequency-locking tongues associated with each rational. All these terms can be given rigorous meanings.

Let us define the sequence w_n as follows:

$$\begin{aligned}
w_1 &= \frac{1}{1+0} = \frac{1}{1} = 1 \\
w_2 &= \frac{1}{1+\dfrac{1}{1+0}} = \frac{1}{1+w_1} = \frac{1}{1+1} = \frac{1}{2} \\
w_3 &= \frac{1}{1+\dfrac{1}{1+\dfrac{1}{1+0}}} = \frac{1}{1+w_2} = \frac{1}{1+\frac{1}{2}} = \frac{1}{\frac{3}{2}} = \frac{2}{3} \\
w_{n+1} &= \frac{1}{1+w_n}
\end{aligned} \tag{18}$$

Another definition of w_n is based on the Fibonacci sequence

$$F_0 = F_1 = 1, \quad F_{n+2} = F_{n+1} + F_n \Longrightarrow 1, 1, 2, 3, 5, 8, 13, \ldots \tag{19}$$

$$w_{n+1} = \frac{F_n}{F_{n+1}} \tag{20}$$

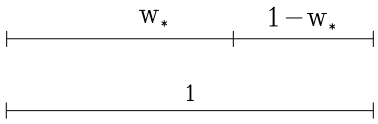

Figure 11: The ratio between $1 - w_*$ and w_* is the same as that between w_* and 1.

These are equivalent, as can be seen from:

$$\begin{aligned} w_1 &= 1 = \frac{F_0}{F_1} \\ w_2 &= \frac{1}{2} = \frac{F_1}{F_2} \\ w_{n+1} &= \frac{F_n}{F_{n+1}} = \frac{F_n}{F_n + F_{n-1}} = \frac{1}{\frac{F_n + F_{n-1}}{F_n}} = \frac{1}{1 + w_n} \end{aligned} \tag{21}$$

The golden mean can be defined by

$$w_* \equiv \lim_{n \to \infty} w_n \tag{22}$$

Definition (18) then leads to

$$\begin{aligned} w_* &= \frac{1}{1 + w_*} \\ w_*(1 + w_*) &= 1 \\ w_*^2 &+ w_* - 1 = 0 \\ w_* &= \frac{-1 + \sqrt{1+4}}{2} = \frac{\sqrt{5} - 1}{2} = 0.618\ldots \end{aligned} \tag{23}$$

The golden mean gets its name from the property illustrated in figure 11, namely that the ratio between $1 - w_*$ and w_* is the same as that between w_* and 1.

$$\frac{1 - w_*}{w_*} = \frac{w_*}{1} \Longrightarrow w_*^2 = 1 - w_* \tag{24}$$

The irrational w_* is the number which is furthest from its approximation by a truncated continued fraction. This implies that it is furthest from its approximation by fractions (because the closest fraction to a number is in fact the truncated continued fraction approximation). Thus the winding number w_* is the irrational furthest from a frequency-locking tongue. A special path through the (Ω, K) plane keeps winding number near w_* and the dynamics away from frequency-locking (i.e. quasiperiodic instead of periodic) as long as possible.

Taylor-Couette flow

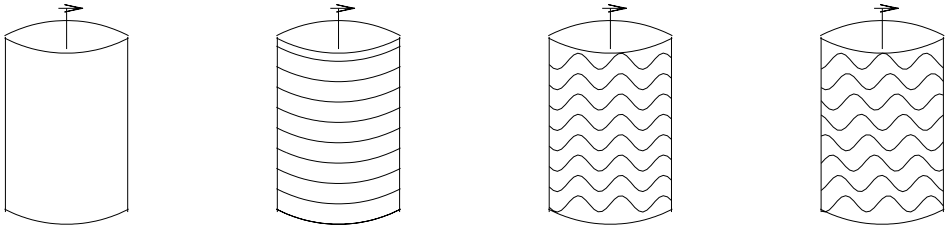

Laminar Couette	Taylor Vortex	Wavy Vortex	Modulated Wavy Vortex
$\mathbf{U}_C(r)$	$\mathbf{U}_{TV}(r,z)$	$\mathbf{U}_{WV}(r,\theta,z,t)$	$\mathbf{U}_{MWV}(r,\theta,z,t)$

Taylor-Couette flow between infinitely long (or very long) differentially rotating concentric cylinders undergoes successive transitions. The transition from *laminar Couette flow* $\mathbf{U}_C(r)$ to axisymmetric Taylor vortex flow $\mathbf{U}_{TV}(r,z)$ is a circle pitchfork, since any phase in z is permitted. The transition to *wavy vortex flow* $\mathbf{U}_{WV}(r,\theta,z,t)$ is a Hopf bifurcation to a limit cycle, since the pattern precesses in θ with time. The transition to *modulated wavy vortex flow* $\mathbf{U}_{MWV}(r,\theta,z,t)$ is a secondary Hopf bifurcation to flow on a torus and introduces another temporal frequency. We have seen above that frequency-locking on a torus is very common as nonlinearity is increased. However, although experimentalists looked for frequency-locking in the 1970s, it was not seen in modulated wavy vortex flow! Why not? In 1981, Rand pointed out that *symmetry* played an important role. Wavy vortex flow, while periodic, is steady in a rotating frame. The time-dependence is on a *symmetry group orbit*: successive states are related by symmetry (rotation) and are hence dynamically equivalent. Saddle-node bifurcations, such as those depicted in figure 4 and 7 cannot occur, since they distinguish between different states (here, values of θ). This explains why frequency-locking is not observed in modulated wavy-vortex flow.

A timeseries from a flow with two frequencies (flow on a torus) is shown in figure 12.

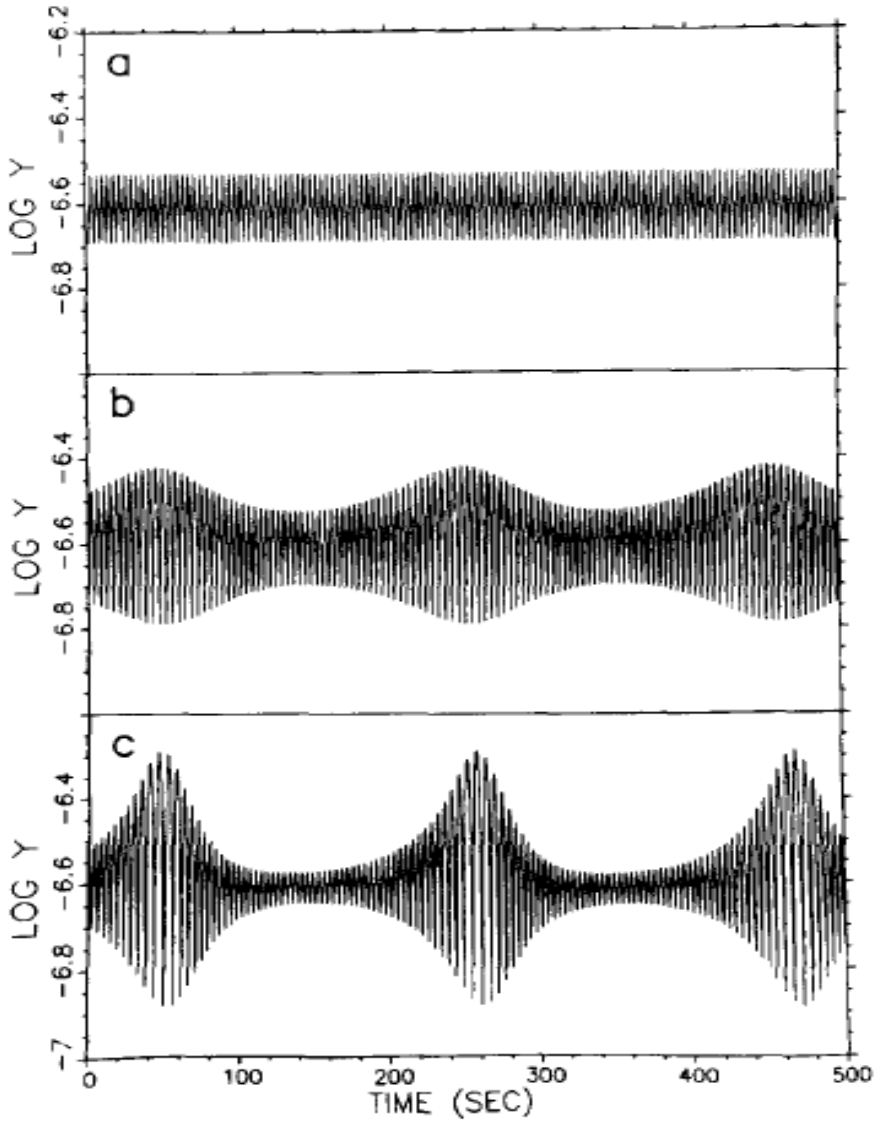

Figure 12: Periodic and quasiperiodic behavior in a model of an oscillating chemical reaction. From D. Barkley, J. Ringland & J.S. Turner, *Observations of a torus in a model of the Belousov-Zhabotinskii reaction*, J. Chem. Phys. **87**, 3812 (1987).

Intermittency

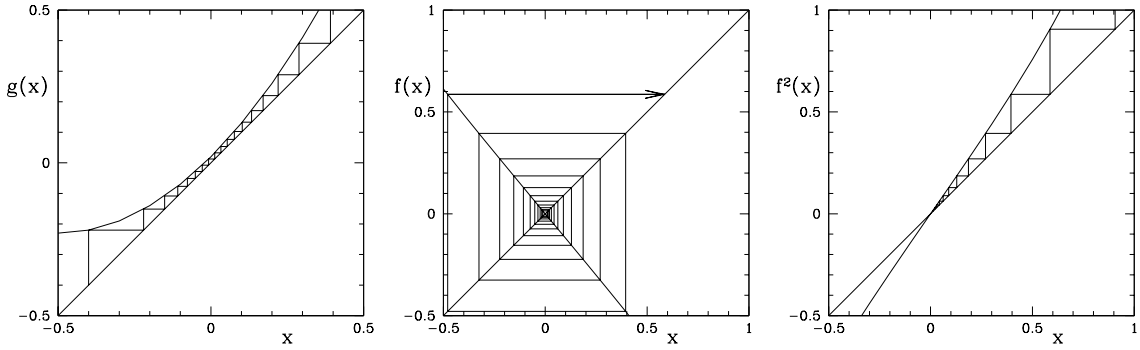

Figure 13: Slow dynamics near a bifurcation. Left: near a saddle-node bifurcation for $g = x_n + 0.2 + x_n^2$, Middle: near a period-doubling bifurcation for $f = -1.2\,x_n + 0.1\,x_n^3$. Right: near a pitchfork bifurcation for f^2.

Intermittency is similar to a phenomenon that we have already discussed, namely slow dynamics near *ghosts* of fixed points close to a *sniper* bifurcation or *saddle-node bifurcation on a limit cycle*.

The left portion of figure 13 shows the iteration of a map

$$x_{n+1} = f(x_n) = x_n - \mu + x_n^2 \tag{25}$$

near a saddle-node bifurcation, both in terms of the initial condition x_0 and also in terms of μ. For $\mu \lesssim 0$, no steady states exist, but the dynamics are slow since steady states $x = \pm\sqrt{\mu}$ exist for $\mu > 0$. It is assumed that another mechanism exists to re-inject the dynamics into the vicinity of $x = 0$. This is called Type I intermittency.

The middle and right portions of figure 13 show the iteration of a map

$$x_{n+1} = f(x_n) = -x_n - \mu x_n + \alpha x_n^3 \tag{26}$$

and of its second iterate $x_{n+2} = f(x_n)$ near a subcritical period-doubling bifurcation for f. Recall that a period-doubling bifurcation for f corresponds to a pitchfork bifurcation for f^2. Both can be supercritical or subcritical. Here too, the dynamics are slow near $x = 0$ and another mechanism is assumed to exist to re-inject the dynamics into the vicinity of $x = 0$. This is called Type III intermittency.

Type II intermittency is associated with a subcritical Hopf bifurcation.

We have seen that the logistic map provides an example of a *route to chaos* via period-doubling. The logistic map also provides an example of a route to chaos via Type I intermittency. The logistic map has a period-3 cycle formed by a saddle-node bifurcation of f^3 at $r_3 = 0.9624$. For $r \gtrsim r_3$, the dynamics visit a period-3 cycle. For $r \lesssim r_3$, the dynamics are chaotic.

Rayleigh-Bénard convection in a small-aspect-ratio container provides examples of all three types of intermittency.

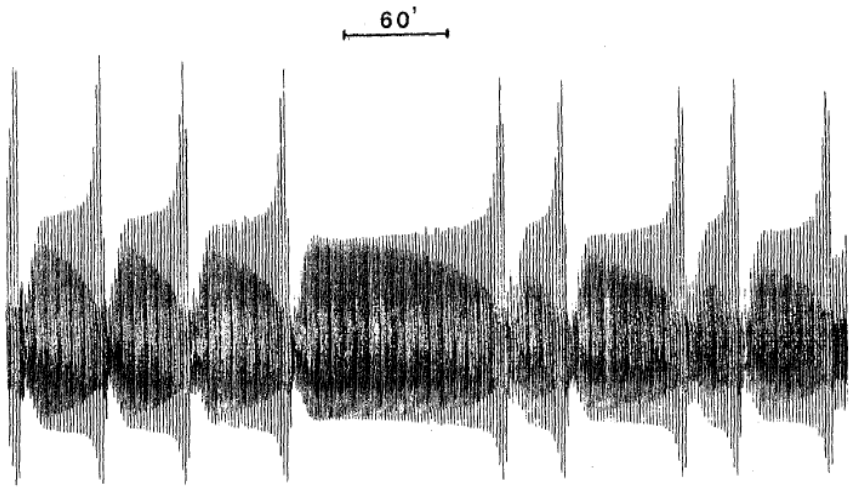

FIG. 1. Time dependence of light intensity, roughly proportional to the horizontal temperature gradient near the cold plume. $N_{Ra}/N_{Ra,c} \approx 420$.

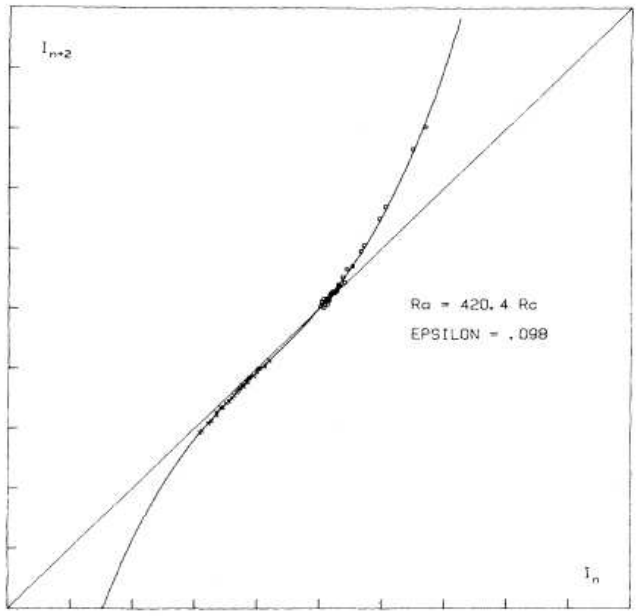

FIG. 2. Return map $I_{n+2} = f(I_n)$, constructed from the data shown in Fig. 1 superposing two laminar periods. The amplitudes of the light modulation in the turbulent bursts have not been drawn.

Figure 14: Type III intermittency seen in Rayleigh-Bénard convection experiment. Top: timeseries. The subharmonic (period-doubled signal) grows, ending with a burst, followed by the laminar phase in which the signal returns to its original period. Bottom: Poincaré map from the maxima of the timeseries $\{I_k\}$ above. The maximum I_{k+2} is plotted as a function of I_k. From M. Dubois, M.A. Rubio & P. Bergé, *Experimental Evidence of Intermittencies Associated with a Subharmonic Bifurcation*, Phys. Rev. Lett. **51**, 1446 (1983).

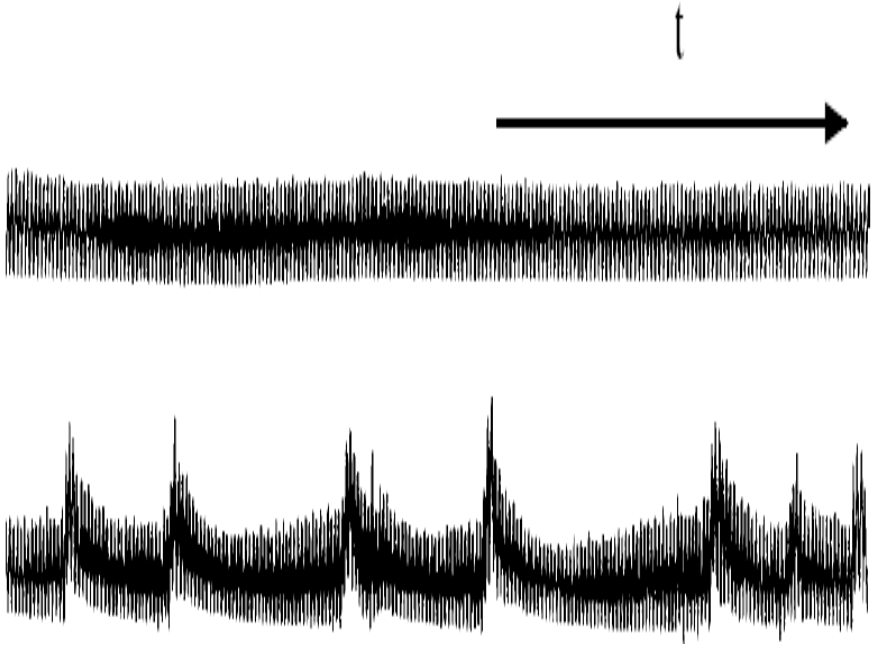

Figure 15: Type I intermittency seen in Rayleigh-Bénard convection experiment. Top: non-intermittent timeseries for $Ra = 280\ Ra_c$. Bottom: intermittent timeseries for $Ra = 300\ Ra_c$. From P. Bergé, M. Dubois, P. Manneville & Y. Pomeau, J. Phys. (Paris) Lett. **41**, 341 (1980).

Lyapunov exponents

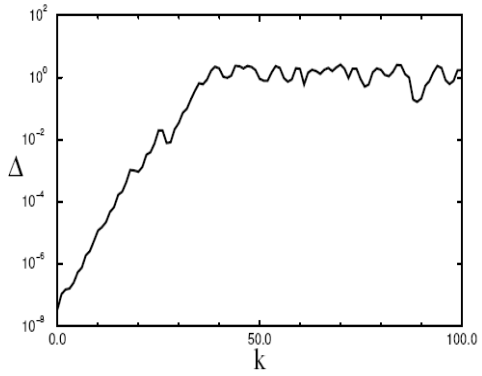

Figure 16: An infinitesimal displacement evolves exponentially until it reaches the attractor boundary. The initial slope seen above is the largest Lyapunov exponent. From P. Manneville, Class notes, DEA Physique des Liquides.

The stability of a steady state $\bar{x}$ is determined by the eigenvalues of the Jacobian matrix. The stability of a limit cycle $\bar{x}(t)$ is determined by its Floquet exponents. Such a quantity can be defined for any kind of attractor and is called the *Lyapunov exponent*. For any trajectory $\bar{x}(t)$, we can study the evolution of an infinitesimal perturbation $\epsilon(t)$, governed by the dynamics *linearized about* $\bar{x}(t)$. The largest Lyapunov exponent is defined to be:

$$\lambda = \lambda^{(1)} = \lim_{t\to\infty} \frac{1}{t} \ln \left| \frac{\epsilon(t)}{\epsilon(0)} \right| \tag{27}$$

In fact, we do not really want to take $t \to \infty$, since once the trajectory reaches the geometric boundary of the attractor, $\epsilon(t)$ ceases to grow. This is illustrated in figure 16. It can be shown that $\lambda^{(1)}$ is independent of the initial condition and characterizes the entire attractor on which $\bar{x}$ evolves. Just as the winding number defines an average rotation per iteration, the Lyapunov exponent defines the average growth or decay per iteration.

The first exponent $\lambda^{(1)}$ is the rate of growth or decay of distances from $\bar{x}(t)$. Rather than monitoring a linear distance ϵ evolving according to the dynamics linearized about $\bar{x}$, we can monitor the evolution of an area. This yields $\lambda^{(1)} + \lambda^{(2)}$, where the second Lyapunov exponent is $\lambda^{(2)}$. One can then define $\lambda^{(3)}$. For a steady state $\bar{x}(t)$, the Lyapunov exponents are the eigenvalues of the Jacobian and for a limit cycle, they are the Floquet exponents.

For a map, we have

$$\epsilon_1 = f'(\bar{x}_0)\epsilon_0 \tag{28}$$

$$\epsilon_n = \prod_{k=0}^{n-1} f'(\bar{x}_k)\epsilon_0 \tag{29}$$

$$\lambda = \lim_{n\to\infty} \frac{1}{n} \ln \left| \prod_{k=0}^{n-1} f'(\bar{x}_k) \right| = \lim_{n\to\infty} \frac{1}{n} \sum_{k=0}^{n-1} \ln \left| f'(\bar{x}_k) \right| \tag{30}$$

On chaotic attractors, nearby initial conditions eventually diverge, and so at least one Lyapunov exponent is positive. This is one of the possible definitions of chaos.

Wrinkling of a torus

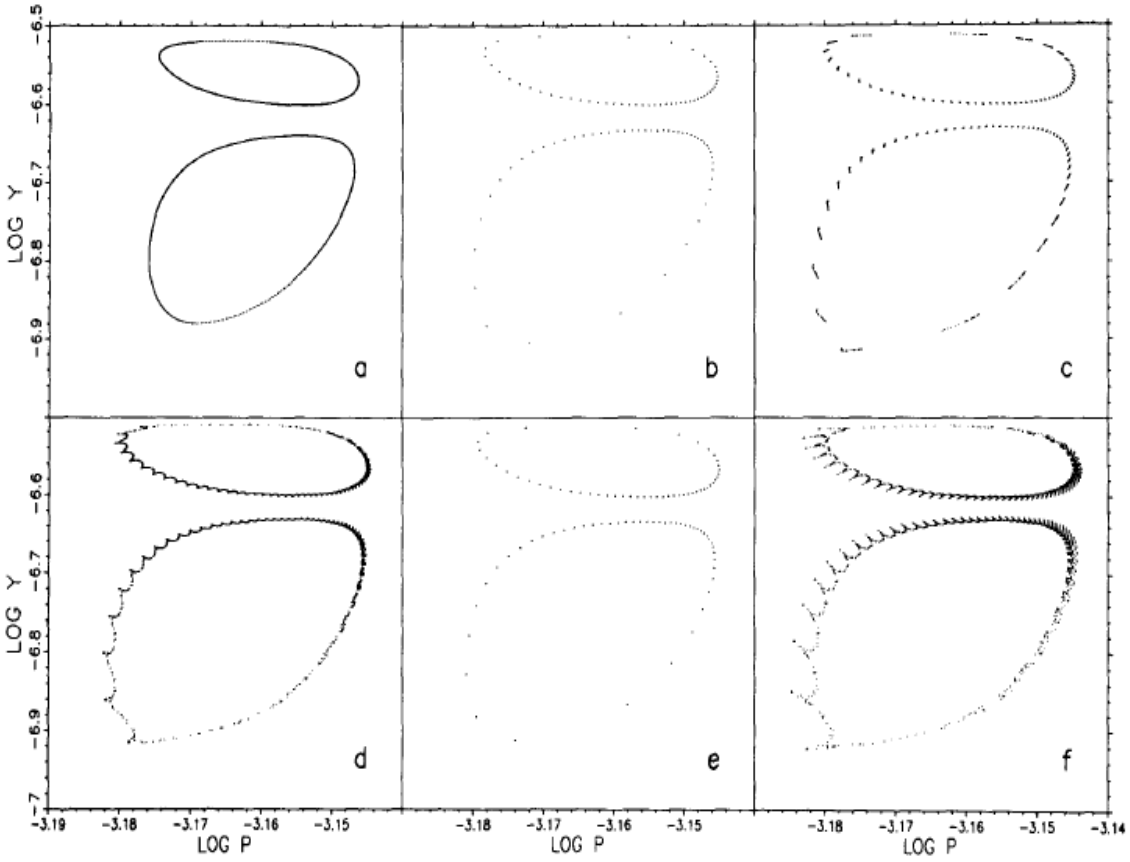

Figure 17: Poincaré sections calculated from a model of an oscillating chemical reaction. One sees quasiperiodic behavior (a), mode-locking (b,e) and wrinkled tori (d,f). From D. Barkley, J. Ringland & J.S. Turner, *Observations of a torus in a model of the Belousov-Zhabotinskii reaction*,J. Chem. Phys. **87**, 3812 (1987).

What happens when K exceeds one? The sine circle map then becomes non-invertible. This implies that:
–it cannot be the Poincaré mapping of a flow
–it can become chaotic (an invertible map cannot become chaotic).

The attractor, which can no longer be mapped onto a circle, may become *wrinkled*, like the example in figure 17.

Route to chaos from a torus

Before the 1970s, the leading dynamical systems theory of turbulence, put forward by Landau, was that turbulence consisted of a sequence of Hopf bifurcations, each adding a frequency to the flow, with turbulence as an asymmptotic state containing a large or infinite number of frequencies. The new developments in the 1970s and 1980s concerning chaos changed this prevailing point of view. First, Lorenz showed that a small set of deterministic ordinary differential equations could lead to behavior that was essentially unpredictable. This was followed by the discovery that only three frequencies could lead to chaos.

More specifically, Ruelle and Takens (1971) and Newhouse, Ruelle and Takens (1978) proved a famous theorem concerning quasiperiodic motion, i.e. motion on a torus, of dimension $n \geq 3$. The theorem says that perturbations could lead to chaos:

"Let v be a constant vector field on the torus $T^n = R^n/Z^n$. If $n \geq 3$, every C^2 neighborhood of v contains a vector field v' with a strange Axiom A attractor. If $n \geq 4$, we may take C^∞ instead of C^2."

How likely are these perturbations? Curry and Yorke (1978) and Grebogi, Ott and Yorke (1985) investigated numerically the probability of random perturbations leading to chaos. Just as the Poincaré mapping for flow on two-torus is a circle map, the Poincaré map for flow on a three-torus consists of a pair of coupled circle maps:

$$\theta_{n+1} = \theta_n + \omega_1 + KP_1(\theta_n, \phi_n) \mod 1 \tag{31}$$

$$\phi_{n+1} = \phi_n + \omega_2 + KP_2(\theta_n, \phi_n) \mod 1 \tag{32}$$

The solutions can be quasiperiodic with three frequencies, quasiperiodic with two frequencies, periodic, or chaotic. The map becomes non-invertible for $K = K_c$. .

Attractor	Lyapunov exponents	$\frac{K}{K_c} = \frac{3}{8}$	$\frac{K}{K_c} = \frac{3}{4}$	$\frac{K}{K_c} = \frac{9}{8}$
Three frequency quasiperiodic	$0, 0$	82%	44%	0%
Two frequency quasiperiodic	$0, -$	16%	38%	33%
Periodic	$-, -$	2%	11%	31%
Chaotic	$+, ?$	0%	7%	36%

(33)